MICROBUBBLE GENERATION BY FLUIDICS.
PART II: BUBBLE FORMATION MECHANISM

Václav Tesař
Institute of Thermomechanics v.v.i., Academy of Sciences of the Czech Republic, Prague

Abstract: In current research project supported by a TAČR grant, author is developing a facility for generation of small, sub-millimetre air sized bubbles in water. This is not easy, the usual bubble size being several millimetres. The most promising and economically viable method, based on author's earlier experience, is fragmentation of bubbles while they are still at the aerator exit locations by a no-moving-part fluidic oscillator. The project involves two major problems discussed separately: (a) developing a suitable no-moving-part oscillator and (b) obtaining a deeper understanding of the effect of oscillation on bubble formation as a pre-requisite to new aerator design. This paper discusses the second problem.

1. Introduction

Bubbles of gas (most often, of course, air) in liquids play essential role in a wide spectrum of various technological processes. Usual aim is to enhance diffusion transport of the gas into the liquid across the interface. Distributing the given gas volume into the very large number of bubbles increases the total interface area, Fig. 1, a key factor in the diffusion transport. The area is larger if the bubbles are smaller; the demand is therefore to make bubbles as small as possible. Recent literature discusses even sub-micron size nanobubbles [3]. These, in theory, can stay suspended in the liquid, agitated by Brownian motion, for time scales as long as days — until they disappear due to the diffusion of all the gas content. Some aspects of nanobubbles are quite controversial (after all, they are not visible by naked eye and even seeing them by a microscope is problematic) and their generation requires a considerable energetic demand. Thus the current goal is a less ambitious one: to produce sub-millimetre sized *microbubbles*.

Apart from the direct advantage of the large overall diffusion transfer surface, the small bubbles also rise to the surface at a much slower velocity, Fig. 2 - so that also the diffusion time aspect leads to an enhanced transport. Bubbles rising to the surface tend to grow by mutual agglomeration. The smaller is the initial size, the longer are even the resultant agglomerate bubbles small and this is another reason for the effort concentrated on the generation of bubbles as small as possible.

The straightforward method how to get the gas into liquid - where it can form the bubbles - is to blow it, under pressure, through orifices in a component called aerator. It is essentially a system of
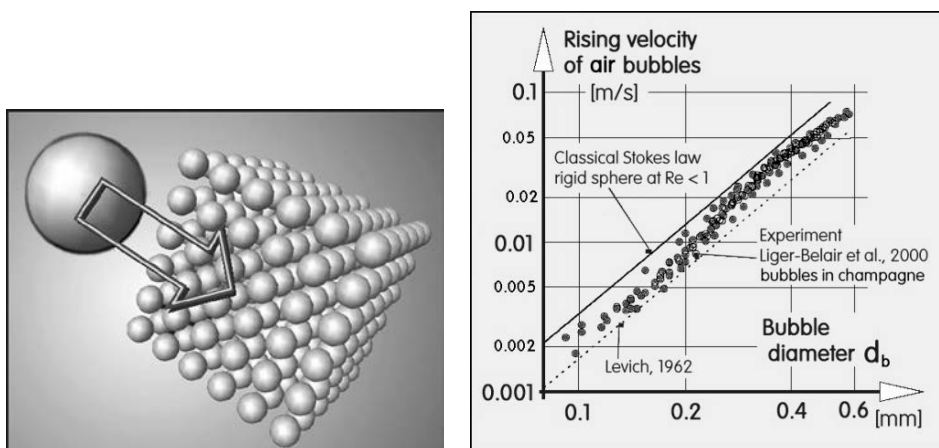
Fig. 1 (Left) Dividing a given volume of gas into a large number of small bubbles increases substantially the overall total surface area across which the gas diffuses into the liquid. This makes more efficient technological processes based on the diffusion.

Fig. 2 (Right) The other effect obtained by making the bubbles smaller is reduction of the velocity with which they rise to the surface [1, 2]. The resultant longer available time for the gas/liquid contact also enhances the diffusion transport.
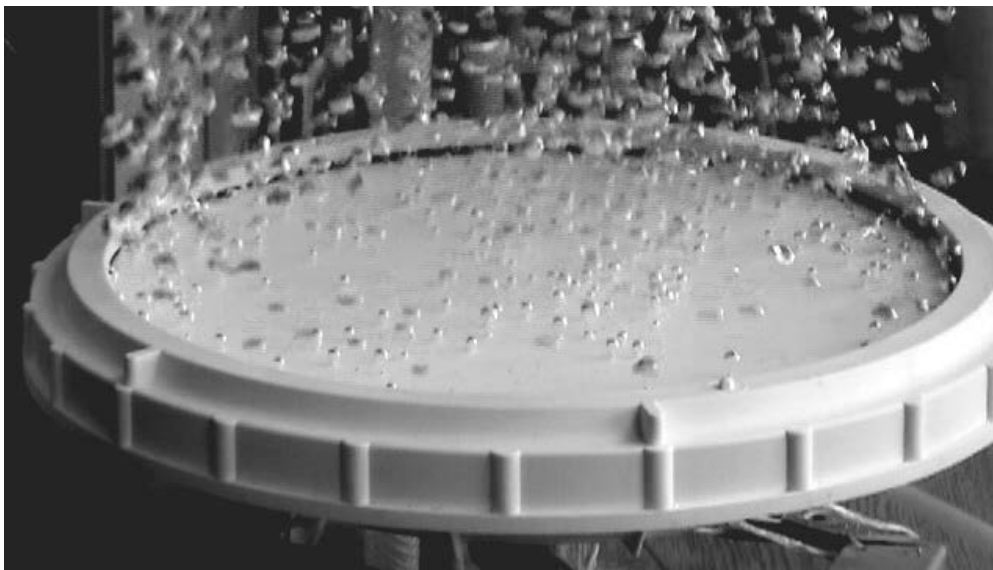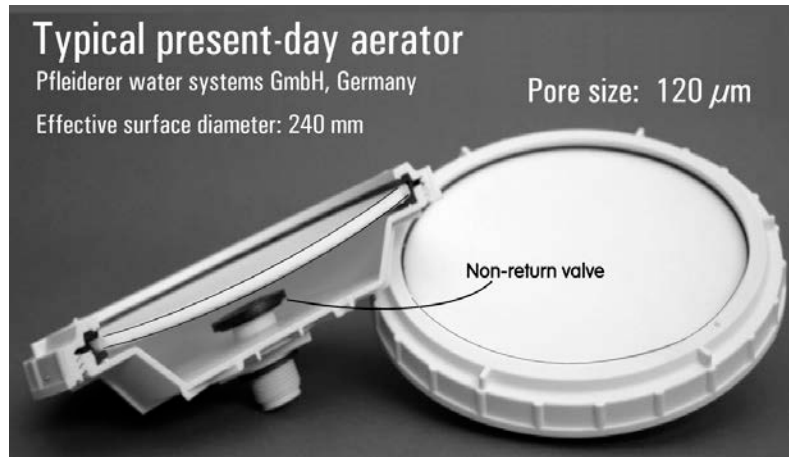
Fig. 3 (Top) A typical aerator as they are currently in use for waste-water treatment. Material: HDPE (High-density polyethylene). The porous top exit surface is made by sintering from very small, sub-millimetre HDPE spheres.

Fig. 4 (Bottom) Author's tests with the aerator from Fig. 3. It is immediately obvious that bubbles are incomparably larger than the membrane pore size: here the average bubble diameter is 5.7 mm (which is 47-times larger than the equivalent pore diameter) in the exit surface.

parallel small orifices leading into the liquid from some larger central inlet space. In an attempt to make the bubbles smaller, it is common to make the aerator exits very small. Unfortunately, this in itself, does not solve the problem. It is a fact, though not generally known, that common aerators produce bubbles an order (and sometimes even two orders) of magnitude larger than the size of exit orifices. A typical example of inadequacy of current aerators in spite of the very small pores is demonstrated in Figs. 3 and 4. The extremely small pores, in this example made by sintering sub-millimetre plastic spheres, obviously do not prevent the bubbles from growing quite large – and only at certain locations on the surface. This is caused by instability of bubble formation, difficult to eliminate since it is a consequence of the very basic law of surface tension.

It is, obviously, desirable to develop new approaches. They do exist, but for one reason or other they are mostly not suitable for the application in industrial processes. On one hand, the method has to be economical. An example of a known but unsuitable solution is generating the micro bubbles by focused laser light. Another method is based on an ultrasound vibrator. The effectiveness of ultrasound transducers is low, making the method applicable to only small scale applications. Another unsuitable approach is use of cavitation in a fast flowing liquid. This can generate very small bubbles, but is associated with large dissipated power levels. Also the surfaces of active components can deteriorate by erosion. A suitable approach is fragmentation of larger bubbles produced by a classical aerator. One

possibility is bubble breakup by shear stresses in turbulent flows. Theory of this approach was set up by Kolmogorov already in 1949, actually for liquid droplets in a gas flow — closely related to the case of bubbles in liquid. In fact some aspects of the fragmentation in the case of bubbles were discussed already in the classical Minnaert's paper on the sound of loquacious water streams [12]. More recently, numerical flowfield computations of the phenomenon were demonstrated in [17]. Nevertheless, setting up of a liquid flow in which the bubbles would disintegrate is rather complicated and also may be quite expensive (from points of views of both energy and finance). Moving components are necessary for moving the water flow and they are inherently susceptible to problems with wear, material fatigue, screws getting lose and so on - so that they generally require maintenance (oiling of bearings, tightening the seals etc.).

A more promising approach was recently introduced in the Patent [7] (also discussed by this author in ref. [18]). It is this case that is the subject of discussion in the present paper. Essentially, it is a fragmentation of sessile bubbles while they still sit at the aerator exits, in the process of their formation. The breakup is to be achieved by oscillation of the air inflow. The mass of liquid does not need to be put into motion; the oscillation is applied in the air inlet, using no-moving-part fluidic oscillators. The applied power is to be relatively very low and there are the advantages of low price, high reliability, long lifetime, and robustness with respect to adverse conditions.

2. Basic law – and instability of bubble formation

Let us first consider the reasons why the aerators currently used, like the one shown in Fig. 4, do not simply distribute the supplied air flow into all small aerator passages and do not produce a large number of very small bubbles. The explanation necessitates considering the basic facts about the interface between gas (air) and liquid (water). Contrary to gases, with their almost independently moving molecules, the liquid molecules ale held closely together by attractive forces (of electrostatic character) acting between them. The forces act on a liquid molecule in a statistically isotropic manner – i.e. the particular molecule is exposed to them from all spatial directions. Forces in every direction are mutually compensated, the molecule is in force equilibrium. This ceases to be the case at the gas/liquid interface. Outside of the interface the molecules are missing. The absent cohesion forces generates results on a force pulling the remaining liquid molecules in the direction away from the interface. The resultant macroscopic effect is a trend to minimise the gas/liquid interface area.

In a bubble this cohesion pull is compensated by pressure difference forces. The pressure inside a bubble is higher than outside to oppose the surface layer force trend to make the bubble smaller. This is represented in Fig. 6. Introduced in this illustration is the coefficient of surface tension σ [N/m]. Its numerical values for various liquids on one side and air on the other side of the interface are presented in Fig. 8. An important fact is that the Young-Laplace law [20] shown in Fig. 6 is equally valid in the case of liquid drops in a gas as it is for gaseous bubbles (Fig. 7) in a liquid. The difference between the two cases is only the fact that bubbles are compressible: their volume may diminish under the action of external pressure applied in the liquid. It should be said that in the processes that are of interest in this paper this compressibility effect may be neglected – the pressure levels are not large enough to deform significantly.

This paper focuses its attention on bubbles in the process of their formation, while they are still attached to the solid wall – surface of the aerator - in which is located the channel bringing into the bubble the supplied air. Relations of a bubble to the solid horizontal surface is characterised according to Fig. 7. It is obvious that the names used there were introduced for the case of drops. They may be pendant (hanging from the ceiling surface above them) or sessile (sitting on the floor surface). This designation will be, as is usual, retained here also for bubbles, although a pendant bubble rather than hanging down is pressed up from below, against the ceiling, because of the inverted (upwards) direction of the acting force (hydrostatic lift rather than gravity). On the other hand, while a sessile drop is stably held by gravity on its supporting wall below, a sessile bubble actually tends to lift off. Computations of bubble or drop shape – as will be shown below in Section 4 – is nevertheless performed using identical equations (and hence identical solution algorithm). The difference is only in the sign of one term in the equations. Nevertheless the tendency of the sessile bubble to move away from its aerator exit at which it was formed is important. Introducing the air through the aerator openings from above into a stable pendant bubble is hardly ever used for aeration. The air bubbles would accumulate under the aerator and would tend to agglomerate there. Thus the desirable goal of producing small bubbles would be practically out of question. Air is usually brought into the aerator (as it is in Fig. 4) from below and the bubbles that are formed are therefore usually of the sessile character. This means the oscillator action on them – the
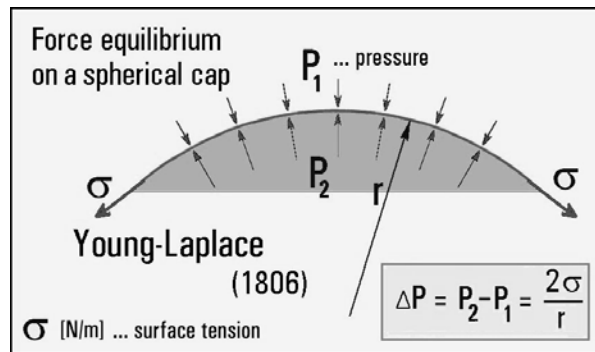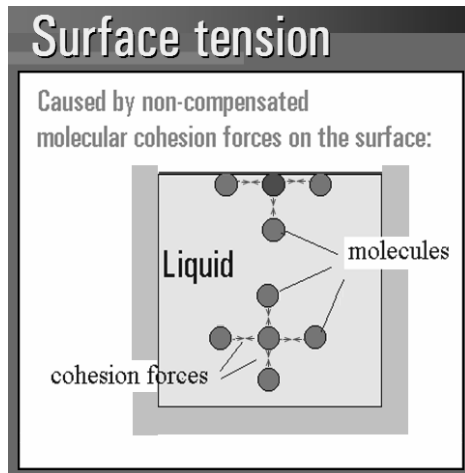
Fig. 5 (Left)   Molecules in liquid are mutually attracted by cohesion forces. For a particular molecule these forces are balanced – they act evenly from all spatial directions so that the molecule is in equilibrium. This balance, is not valid for the molecule at the liquid surface: there is a net resultant force pulling these molecules towards the liquid half-space where there is a higher pressure than in the gas outside.

Fig. 6 (Right)   The liquid/gas interface is governed by the Young-Laplace law [20] for the pressure that compensates the pulling action of the surface. The law says the curvature radius of the interface is inversely proportional to the pressure difference. The proportionality factor is a property of the particular combination of gas and liquid and is characterised by the value of the surface tension σ.
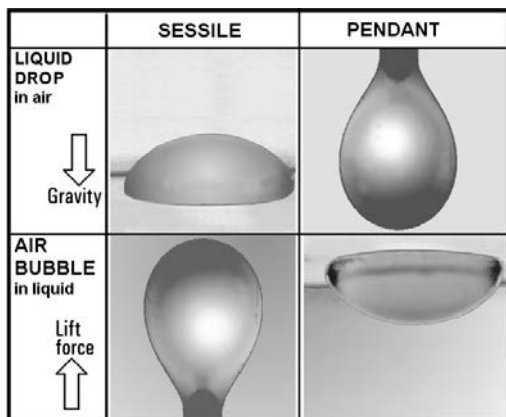
Pure liqid/air interface surface tension		
	Temperature	Surface tension
Liquid	°C	mN/m
Acetone	25	24.0
Aniline	20	42.7
Benzene	20	28.9
Benzonitrile	20	39.4
Blood	37	33.5-61.2
n-Butane	20	12.5
Carbon disulfide	20	32.3
Carbon tetrachloride	15	27.7
Chlorobenzene	20	33.6
p-Cresol	40	34.9
Cyclohexane	20	25.2
Diethyl ether	15	17.6
Diesel Fuel Oil	20	26.2
Ethanol	40	21.38
Ethyl acetate	20	24.0
Glycerol	20	63.4
n-Heptane	20	20.1
Mercury	25	483.5
Methyl alcohol	20	22.6
Phenol	40	39.3
n-Propyl alcohol	20	23.7
Pyridine	20	37.2
Saliva	37	53.0
Water	25	72.3

Fig. 7 (Left)   Equivalence of the surface effects acting on gas bubbles and on liquid drops. These objects at a solid wall may be pendant (hanging from top, although in the case of a bubble it is actually pressed against the ceiling surface) or sessile - sitting on the bottom.

Fig. 8 (Right) Numerical values of the surface tension σ as the proportionality factor in the Young-Laplace law: the case of air bubbles in various liquids.
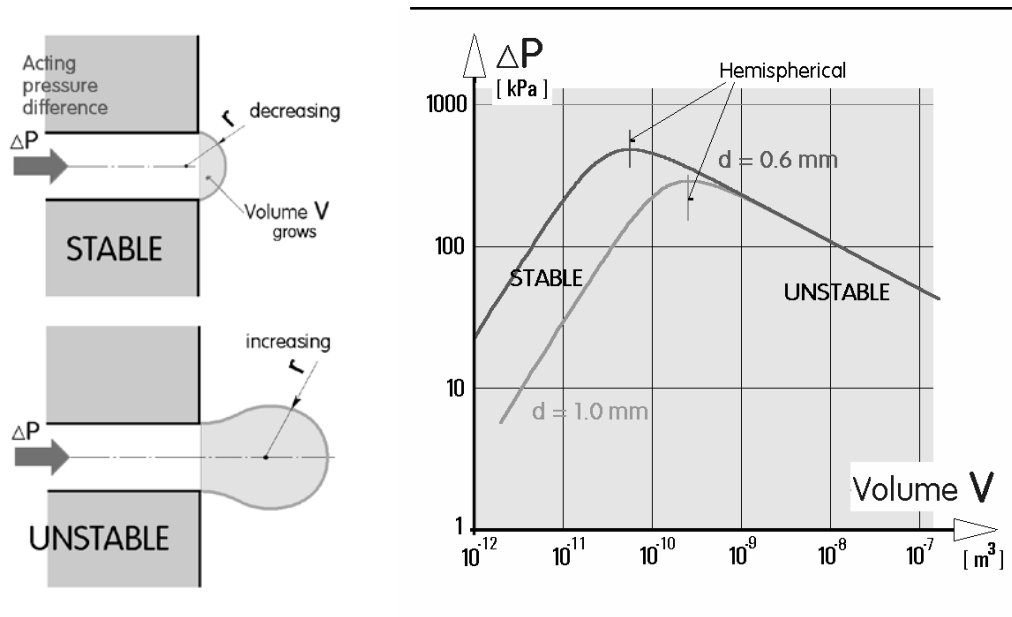
Fig. 9 Two stages of formation of an air bubble at the exit from an aerator orifice are shown at left. In the initial stage, as shown on top, the increase in the bubble volume decreases the curvature radius r and this is associated with increase of pressure difference. This stable stage is represented by the upwards sloping part of the diagram, which shows two computed examples (for different aerator exit diameters d) of the pressure dependence on the volume of growing bubble. In the second stage, shown at left bottom, the situation changes dramatically: the bubble growth becomes unstable as is represented in the diagram by the downwards sloping part of the dependence.

subject of the current research project - is more difficult, since the oscillation applied to cause fragmentation may tend to cause separation of the bubbles from the sessile attachment surface and moving them away.

Let us now consider the case of growing bubble in the exit of an aerator channel as it is shown in the left-hand side of Fig. 9. There are two stages of the bubble growth. In both the gas is supplied under pressure and this causes the volume of the bubble to increase. At the beginning of bubble formation, the curvature radius of the gas/liquid interface is infinite (the interface is a flat plane). With the progressing gas supply the curvature radius gradually decreases. This is the first stage. Obeying the Young-Laplace law, the pressure difference across the interface (inversely proportional to the radius) must increase. This is a stable situation. Let us assume the gas inflow stops for a moment and consider the stability of the ensuing equilibrium. If the pressure inside the half-bubble decreases - due to some disturbance - the consequent decreased volume means an increase of the radius r and according to the Young-Laplace law the pressure difference across the interface would increase. The pressure force would return the bubble into its equilibrium state. The law acts against any change, the bubble is stable. Graphically is this dependence presented in the diagram (results of author's computations for two examples with different inlet channel diameter d) on the right-hand side of fig. 9. The positive slope, valid for the radius r larger than one half of the diameter d represents a stable equilibrium.

This is, however, valid only as long as the growing half-bubble does not reach the hemispherical shape. In the subsequent second stage of the bubble growth, shown in Fig. 9 in the bottom part at left, the bubble radius increases with increasing bubble volume. This is associated with diminishing pressure difference ΔP. The lower pressure inside the bubble makes possible inflow of additional gas. This means an increase of the curvature radius r and further decrease of the pressure difference ΔP. There is no mechanism that would restrict the growth – apart, perhaps, from the hydraulic loss in the channel supplying the compressed air. The slope in the diagram shown at right in Fig. 9 becomes in this second stage negative. The bubble growth is unstable.

Consider now the case of a simple but typical aerator presented in Fig. 10, with the usual several parallel exits. These form a row of identical passages between the water-filled space and the common horizontal manifold, into which is pushed the supply air flow. The planar top surface of the aerator body
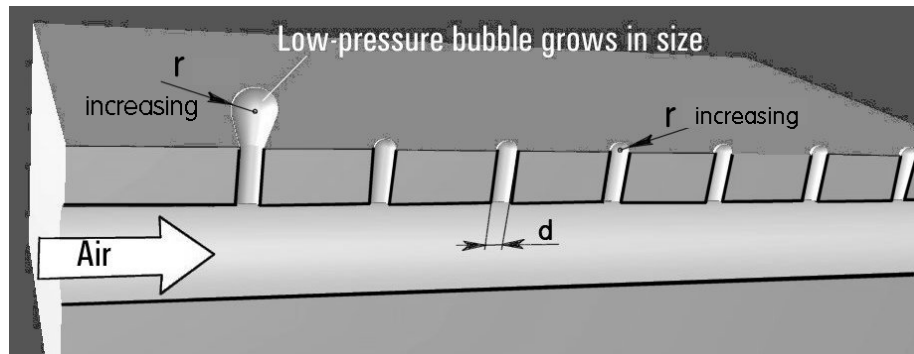
Fig. 10   Parallel formation of bubbles supplied from a common air inlet manifold. Initially all bubbles have curvature radius larger than d/2 and they all grow. As soon as one of the bubbles transgresses the hemi-spherical shape limit, the Young-Laplace law causes fast growth in this bubble (r increasing). This, however, happens at the expense of its neighbours, which may reverse their initial growth. Their curvature radius r are then also increasing, but in a different context of return to the planar shape of the interface.

represents the bottom floor to which are attached the formed bubbles. As we shall see, the distribution of air flow into the bubbles growing in parallel is initially stable – but later enters the unstable stage.

Initially, the surface curvature radius r , in a similar manner as in the top left part of the previous Fig. 9, is larger than one half of the passage exit diameter d. As in Fig, 9, the bubble growth is steady, the air flow is distributed evenly from the manifold into all vertical passages. Of course, not all passages can be made absolutely identical and one of them is bound to reach earlier the hemispherical critical regime. This gives to this bubble instantaneously a strong advantage over its neighbour bubbles. Once this first bubble enters the unstable region its radius of surface curvature becomes larger and consequently (according to Fig. 6) the pressure inside this bubble decreases. This decrease make possible uncontrollable additional growth - with increasing large radius of the preferential bubble while curvature radii of other bubbles are smaller. They may not only stop growing but the higher pressure acting on the interface can even cause retreat of the air back into the exit passage. The result corresponds to what is demonstrated in the example in Fig. 4. Though not visible in the photograph, there are in the aerator exit surface in Fig. 4 many extremely small passages – membrane pores. Most of them are visibly passive – not engaged in bubble formation, even though they provide also an open way for the air into the liquid. The supplied air passes through the few preferential pores and due to the instability of parallel bubble formation the bubbles in these preferential positions grow out of all proportion to the pore size.
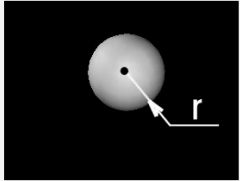
3. Surface energy point of view

It is also possible to view and interpret the behaviour of the bubbles in a different context. This is presented in Fig. 11. It is an approach based upon the idea of surface energy. Energy is a capability to perform some work and the work in this case is the one that has to be to be done when a new liquid/gas interface is created, as is shown in Fig. 12. A liquid column there is imagined to be cut in half and the two halves are then separated form one another. This cutting and separation is inevitably associated with disrupting some of the cohesion forces between the molecules inside the liquid, according to Fig. 5. If the
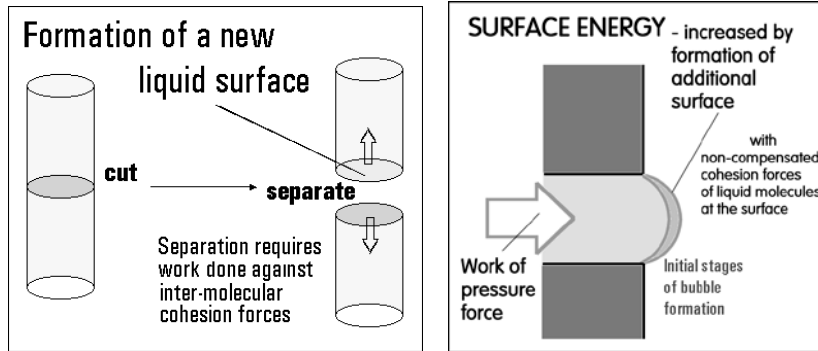

Fig. 11 There is another viewpoint on the behaviour of the gas/liquid interface. It expresses the phenomena in terms of the surface energy. The surface tension σ   (same as in Figs., 5 and 7) in this case specifies the amount of the energy per unit area of the surface.

Fig. 12 (Left) The idea of surface energy is based upon the notion of work that is to be done when a new interface is created, which is associated with disrupting the cohesion forces between the molecules of the liquid.

Fig. 13 (Right) The concept of surface energy applied to formation of a bubble. Even though there is not the cutting and separation operation form Fig. 12, the very increase in size of the growing bubble is associated with increasing number of the liquid molecules near the boundary whose cohesion forces are not balanced because there are no neighbour molecules outside the interface.

liquid is given a suitable opportunity, it will tend to unite again into a single body of liquid and renew the severed cohesion action. On doing this re-union, the liquid is prepared to perform some mechanical work. This means that in the separated state it possessed some energy – capability to work. This energy is directly proportional to the size of the interface and as shown in Fig. 11, the coefficient of proportionality is the surface tension σ of the Young-Laplace law (note the identity of dimensions: $N/m^2 = J/m^2$).

The surface energy approach may be also usefully applied, with the starting point as shown in Fig. 13, to the problem of instability in the bubble formation discussed above in terms of the forces rather than energy. The really strong point of the energy approach, however, is the evaluation of the problems associated with disintegration of bubbles and the fragmentation. It may directly lead to answering the questions of the necessary power needed for the bubble breakup. Let us here consider simple situations – like the one in which a bubble or drop of radius r is forced to break in two daughter objects. Each of them has radius r_2

$$r_2 = 2^{-1/3} r$$

This increases the total surface area to $\quad F_2 = 2 * 4\pi (2^{-1/3})^2 r^2 = 2^{7/3}\pi r^2$

and the total surface energy increase is easily evaluated as $\quad E_2 = 2^{7/3}\pi r^2 \sigma$

This is an important fact: splitting a larger bubble into two smaller ones is associated with an increase of total energy. The increase is the difference
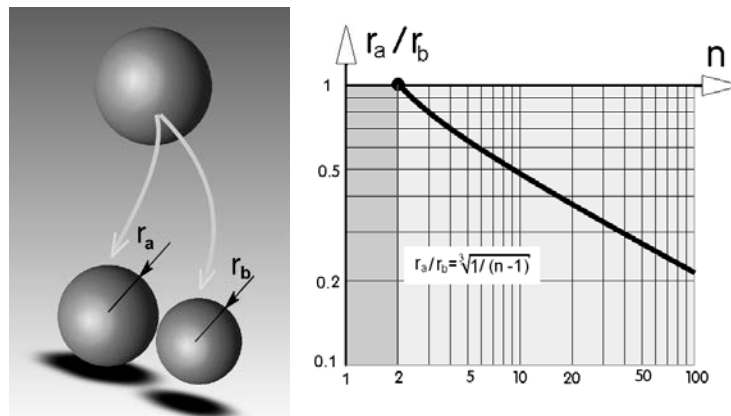
Fig. 14 Consider a bubble divided into two daughter bubbles, the smaller satellite drop containing the n-th part of the original volume. The diagram at right shows the ratio of the daughter bubbles radii for various n. The pictorial representation at left is drawn to scale for the case n = 3, i.e. the satellite containing one third of the original volume.

Of course this increase in energy must be supplied from some source. In the investigated case of fluidic fragmentation this energy must come from the fluidic oscillator. It may be useful to consider the energetic effect in an context of a moving drop that is suddenly stopped

The original drop had volume

$$V = 4 \pi r^3 / 3 \text{ and mass } M = 4 \pi r^3 / (3 v).$$

The change of energy ΔE represents the deceleration to still-stand from a motion with kinetic energy

$$\Delta E = 0.5 M w^2$$

i.e. from the original velocity $w = (2 \Delta E / M)^{1/2} = (2* 2^{1/3} * 3 v \sigma / (4 r))^{1/2} = (2^{-2/3} * 3 v \sigma / r)^{1/2}$

This may be compared with the velocity of the applied fragmentation oscillation

It is a general fact that bubbles (or liquid drops, for that matter) are rarely split into two bubbles of equal volume. Much more often encountered situation is separation from a larger bubble of a smaller one. This is described as satellite. Satellites are cause of problems in several technological processes, because they may be formed with rather small applied work. Typical significant problems are encountered in producing metallic spheres for sintering [21]. Another situation in which spontaneously generated satellite droplets are a cause of troubles are inkjet printers. Because of their different aerodynamic and ballistic properties, satellites cause degradation of printing quality [19].

Let us assume a drop of volume $V = 4 \pi r^3 / 3$ divided onto the daughter drop (a) and its satellite (b), the latter containing the n-th part of the original volume.. Their volumes after the split are

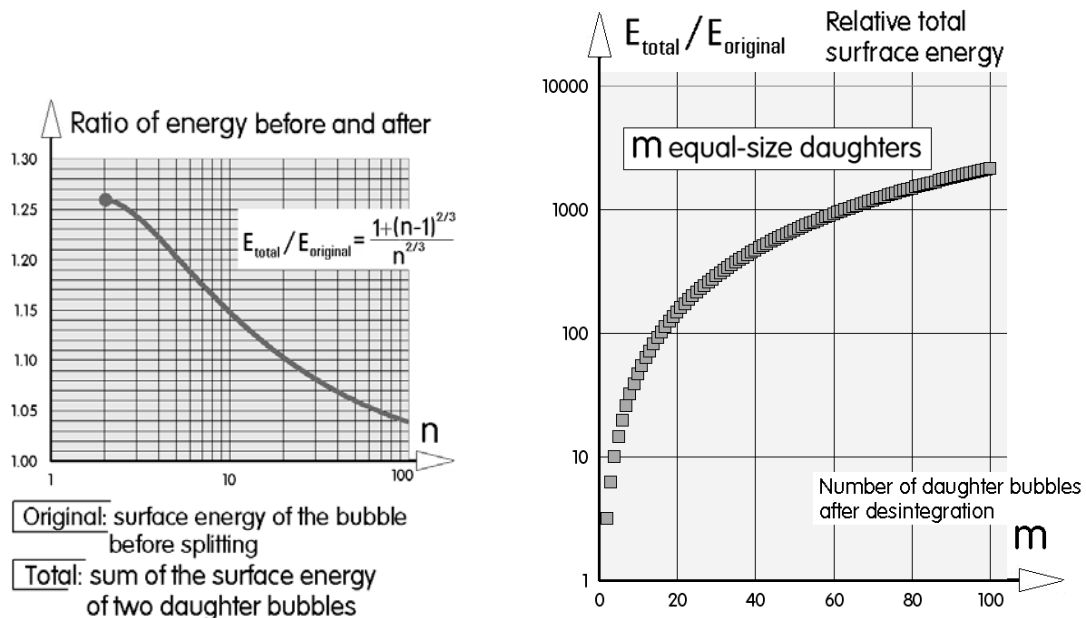$$V_a = 4 \pi r^3 / (3 n) \qquad \text{and} \quad V_b = 4 \pi r^3 (n-1) / (3 n)$$

The corresponding radii are $\qquad r_a = \sqrt[3]{(3V_a/(4 \pi))} = r \sqrt[3]{(1/n)}$

and $\qquad\qquad\qquad\qquad\qquad r_b = \sqrt[3]{(3V_b/(4 \pi))} = r \sqrt[3]{((n-1)/n)}$

Diagram in Fig. 14 presents the ratio $\qquad r_a / r_b = \sqrt[3]{((1/n)/((n-1)/n))} = \sqrt[3]{1/(n-1)}$

Surfaces of the two drops are $\qquad F_a = 4 \pi r_a^2 = 4 \pi r^2 * \sqrt[3]{(1/n^2)}$

$$\text{and} \qquad F_b = 4 \pi r_b^2 = 4 \pi r^2 * \sqrt[3]{((n-1)^2/n^2)}$$

Fig. 15 (Left) The daughter bubbles (the satellite as well as the rest) after the division in Fig. 15 have larger total surface than the original single bubble. Thus the split into two is associated with increase in total surface energy and this (roughly) represents the work that has to be done to achieve the division.

Fig. 16 (Right) A different case: energy increase by fragmentation of a large original bubble (according to Fig. 1) into m smaller bubbles, all of them of equal size.

Total surface ⬜ of the drops after the satellite is formed is

$$F_{total} = 4 \pi r^2 * [\sqrt[3]{((n-1)^2/n^2)} + \sqrt[3]{(1/n^2)}] = 4 \pi r^2 \; n^{-2/3} * [1 + \sqrt[3]{(n-1)}]$$

The original surface was, of course, $F_{original} = 4 \pi r^2$

This means the formation of the satellite increases the surface area by $\Delta F = F_{total} - F_{original}$

$$= 4 \pi r^2 (n^{2/3} * ([1 + \sqrt[3]{(n-1)^2}]) - 1)$$

Ratio of surfaces is $\qquad F_{total} / F_{original} = n^{-2/3} * [1 + \sqrt[3]{(n-1)^2}]$

- and this is also equal to the ratio of total and original surface energy magnitudes in Fig. 15. Obviously, the energetically most demanding is the split into two halves, $n = 2$. The smaller is the satellite (i.e. the higher is the vale n) the less energy is required for the satellite formation – which explains the above already mentioned frequent occurrence of small satellites.

      Of particular importance in the context of the bubble fragmentation project is the energy increase evaluation in the case of a single original bubble disintegrated into m daughter bubbles of equal curvature radii r_d of their surface. The ratio of the resultant larger total surface energy

$$E_{total} = m \; 4 \pi r_d^2 \sigma$$

to the surface energy of the single bubble $E_{original} = 4 \pi r^2 \sigma$ is

$$E_{total} / E_{original} = m (r_d / r)^2$$

Because of the condition of equal volumes

$$4 \pi r^3 / 3 = m \, 4 \pi r_d^3 / 3$$

$$(r_d / r)^2 = m^{2/3}$$

the energy ratio is $\qquad E_{total} / E_{original} = m^{5/3}$. As may be seen from the presentation of this result in Fig. 16, a disintegration of each bubble at an aerator exit into, e.g., 20 small bubbles requires in an ideal case an amount of work roughly 150-times larger than the formation of the larger bubbles. Of course, this is the least estimate of the power to be applied. The effectiveness of the fragmentation device being less than 100 %, the actual power will be considerably higher.

4. Basic bubble shapes

      The estimates presented above were based upon the simplifying assumption of the bubbles being of spherical shapes. This is the shape of bubbles freely moving in the liquid. However, both sessile and pendant bubbles (as well as drops) are of more complex shape. To evaluate their aspherical geometry, it is necessary to apply a more general version of the Young-Laplace law, according to Fig. 17 operating with the principal radii. There is a point on the bubble surface with both principal radii equal. This is the apex point (the point most distant from the attachment plane) . The two identical principal radii there are equal to the apex radius r_A . In a general point on the drop or bubble surface (Fig. 18 shows the sessile drop case) the surface arc is locally osculated by a circle in the meridian plane the radius of which is the first principal radius r_1. Fig. 18 also introduces the Cartesian co-ordinates measured from the apex. The second principal radius r_2 is equal to $X_1 / \sin \varphi$ where X_1 is the radial Cartesian co-ordinate, The pressure difference in the Young-Laplace law equation may be expressed for a general surface point as the sum of the pressure difference in the apex plus the hydrostatic pressure increase between the apex and the particular point.

      For the apex

$$\boxed{\Delta P_{apex} = \frac{2\sigma}{r_A}}$$

In the hydrostatic difference term in the next Fig. 19 the specific volume $v_a \, [m^3/kg]$ is that of and $v_w = 10^{-3} \, m^3/kg$ is the specific volume of water, while $g \, [m^2/s]$ is the magnitude of the gravity acceleration. The next derivation step is presented in Fig. 20. Using the expression for the slope

$$\frac{dX_3}{dX_1} = tg \varphi$$
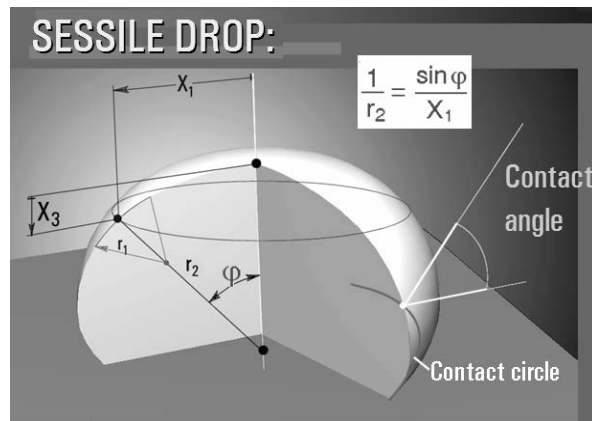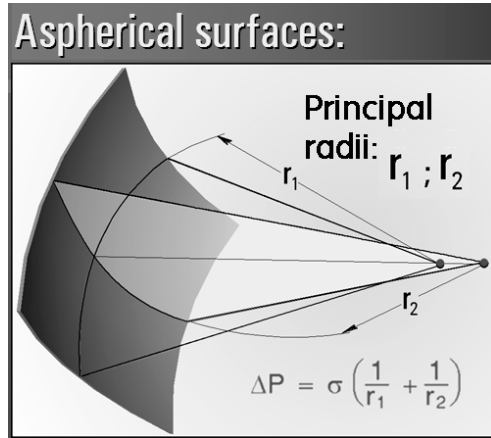
Fig. 17 (Left) Generalised form of the Young-Laplace law for surfaces having more complex (not spherical) shape of their surface: the law is expressed by means of the principal radii.

Fig. 18 (Right) The concept principal radii applied to computation of shapes of sessile drops – or to pendant bubbles. As was already shown in Fig. 6, the bubbles and drops at solid surfaces are aspherical.

and the standard expression for curvature radius, this picture writes the result as two differential equations of first order, using as the parameter the inclination angle φ of the drop surface relative to the horizontal. In the next Fig. 21 the two equations are non-dimensionalised by introducing the useful auxiliary variable – capillary length l_{cap}

$$l_{cap} = \sqrt{\frac{\sigma}{g/v_w - g/v_a}}$$

and the three dimensionless variables

$$x = X_1/l_{cap}$$

$$y = X_3/l_{cap}$$

$$p = \frac{\Delta P_{apex}}{\sigma} l_{cap}$$

Because the capillary length depends only on properties of the gas and liquid (and on gravity acceleration), it may be useful to evaluate its numerical magnitude for the most important case of ware and air. The specific volume of the latter is $v_a \, [m^3/kg] = r \, T / P$ (where T – temperature, P – pressure,

Fig. 19 (Left) The asphericity is due to the differences of hydrostatic pressure along the bubble (or drop) height. The expression of the hydrostatic pressure difference is inserted into the law from Fig. 17.

Fig. 20 (Right) Further development of the equation from Fig. 19 into two first-order non-linear differential equations.
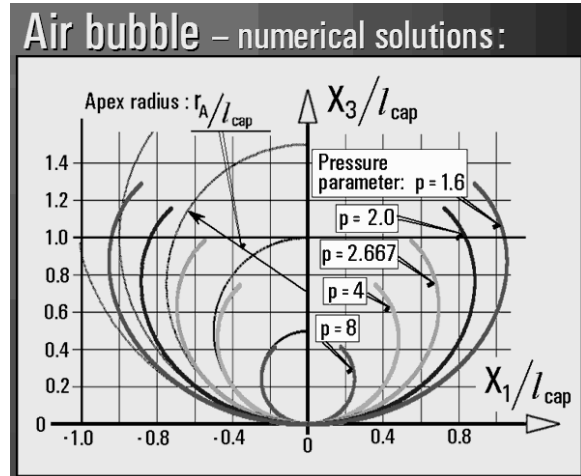
Fig. 21 (Left)   By introducing dimension-less variables the two equations from Fig. 20 are given a simpler appearance – and universal validity.

Fig. 22 (Right) Results of the numerical integration of the equations from Fig. 21 for five different values of the pressure parameter p.

and the gas constant r for humid air r = 288 J/kgK), specific volume of water $v_w = 10^{-3}$ m^3/kg and g = 9.81 m^2/s, so that for the usual laboratory conditions the capillary length of water/air interface is
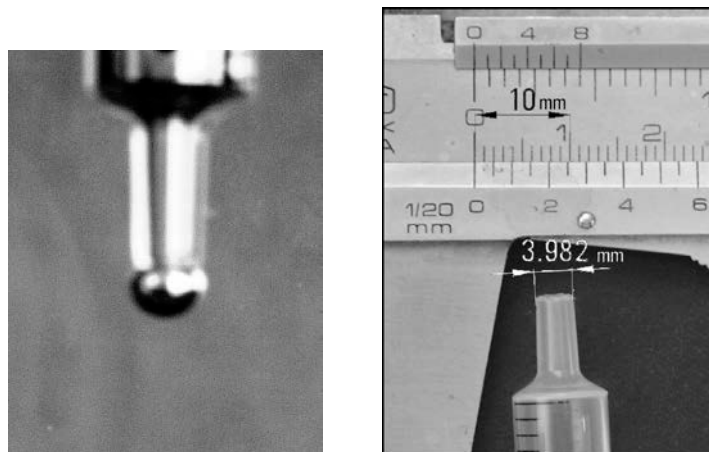
$$l_{cap} = 2.72 \text{ mm}$$

The result of the non-dimensionalisation are two nonlinear ordinary differential equations of the first order, with parameter p :

$$\frac{dx}{d\varphi} = \frac{x \cos\varphi}{xy + xp - \sin\varphi}$$

$$\frac{dy}{d\varphi} = \frac{x \sin\varphi}{xy + xp - \sin\varphi}$$

Five examples of the numerical integration of these two equations for the case of pendant air bubble in water and various values of the parameter p are presented in Fig. 22. Author has compared the

Fig. 23 (Left)   Author's photograph of an air bubble formed in a water-filled fish tank at the tip pf a syringe. The shape of the bubble was compared with the solutions presented in Fig. 22.

Fig. 24 (Right) Dimensions of the syringe tip used in Fig. 23 were evaluated from the microphotograph taken together with a caliper rule.
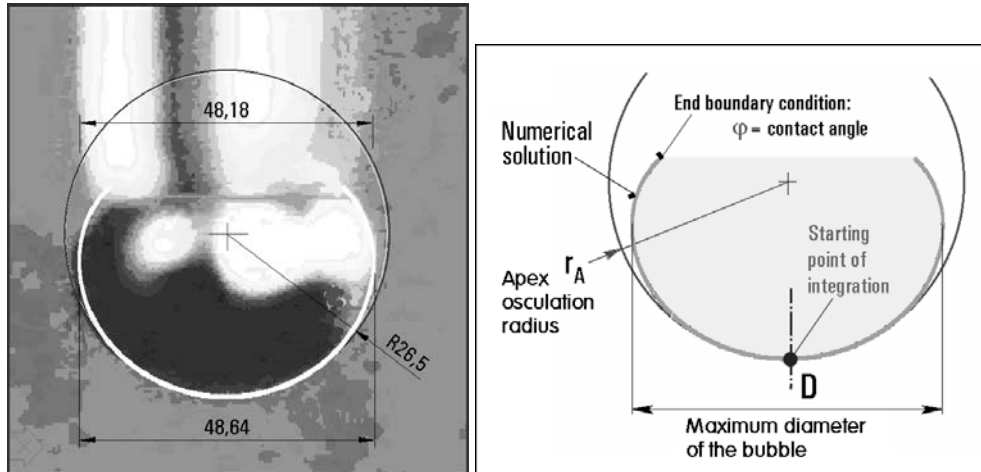
Fig. 25 (Left) Magnified photograph of the air bubble from Fig. 23 with the evaluated dimensions (in pixels).

Fig. 26 (Right) The solution of the non-linear differential equations from Fig. 21 for the pressure parameter p fitted to the shape of the bubble surface. This makes possible evaluation of the capillary length, defined in Fig. 21, and from this – for known specific volumes of water and air – finding the numerical value of surface tension σ which may differ from the value given in Fig. 8 due to the dependence on temperature and, more significantly, due to contamination by surface agents.

the results of this computation with a simple experiment, made during his stay at the University of Sheffield, in the course of which air bubbles were formed and photographed – as shown in Fig. 23 - under the water surface in a fish tank (fish were absent) at the tip of a small standard syringe (without the hypodermic needle). The syringe tip is also shown in the photograph Fig. 24, which served for evaluation of the exit diameter. The agreement – Figs. 25 and 26 – is so good it were possible to use such simple experiment for evaluation of the surface tension σ (which, mainly because of various contaminations, in real experimental conditions may differ from the value presented in Fig. 8 and usually assumed valid without checking in aerator tests).
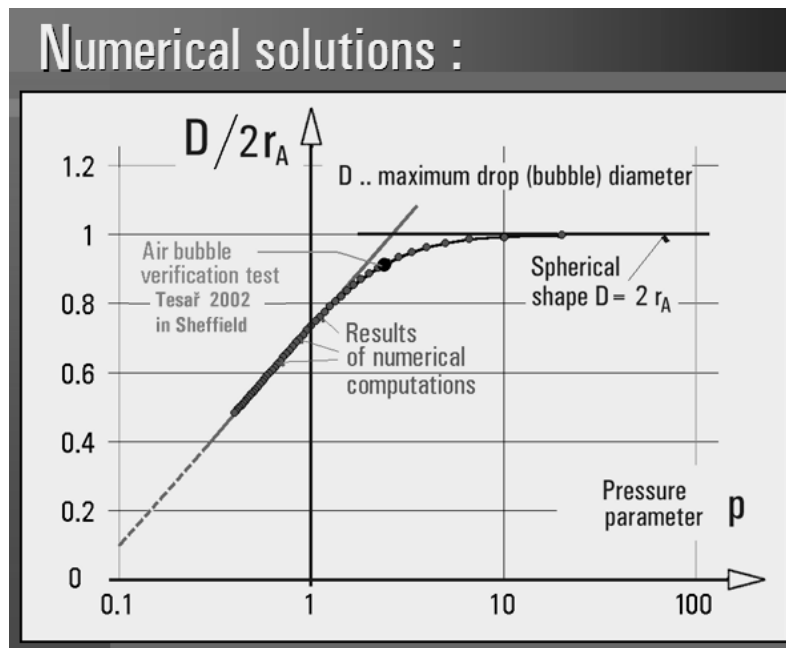
Fig. 27 Author's series of numerical solutions of the equations from Fig. 21 resulted in this dependence of the parameters of bubble shape factor - the ratio of maximum bubble diameter to its apex osculation radius – on the pressure parameter.
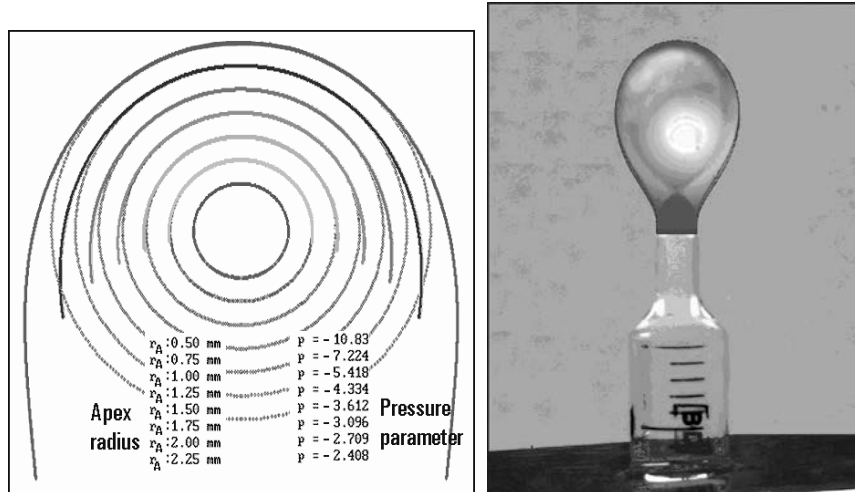
Fig. 28 (Left)   Results of numerical computations: the equations from Fig. 21 are integrated with negative values of the pressure parameter p. The shapes correspond to the sessile bubbles (or pendant drops).

Fig. 29 (Right) An example of sessile bubble made by blowing air into the fish tank by a syringe through the sealed hole in the tank bottom. The sessile bubbles are rather unstable and generating shapes like the one shown in this illustration is rather tricky (this particular bubble was in fact not really stationary and was photographed just before its lift-off separation).

The asphericity of bubbles is seen from the solutions in Fig. 22 as the difference between the computed meridian shape and osculation circle passing through apex point. The difference is particularly well visible in Fig. 26 which shows the geometry fitted to the conditions of the experiment from Figs. 23 and 25. The value of the pressure parameter there was p = 2.667. The difference gradually disappears (so that the shape of the bubble becomes practically identical to the apex osculation sphere) at high values of the pressure parameter p. In Fig. 22 the difference may be described as negligible for the value p = 8. A useful measure of this difference is the ratio $D / 2 r_A$ - where D is the maximum diameter of the bubble and r_A is the radius of the apex osculation circle. In the experiment according to Figs. 22, 23, and 25 the value of this ration was $D / 2 r_A = 0.9177$. Evaluated by the author from large number of numerical solutions of the equations from Fig. 21 with different pressure parameter values are the data plotted in Fig. 27. In the semi-logarithmic co-ordinates there are two asymptotes: the spherical shape asymptote for the very large p > 8 while the other asymptote approach the strongly aspherical cases.

As was already mentioned, the same two equations from Fig. 21 are used for evaluating the shape of sessile bubbles. The example solutions are presented in Fig. 28. Again, with shape approach sphericity at large absolute values of the pressure parameter and the numerical data for air/water interface show that the microbubbles to be generated in the current project will be practically spherical.

4. Oscillatory deformations leading to fragmentation

In an overwhelming percentage of references in available literature, the bubble oscillation processes that have been studied were the pulsation of the bubble radius made possible by air compressibility – while the bubbles retained their symmetric shape. The differential equation describing these oscillation were derived already in 1917 by Rayleigh [11]:

$$ r\ddot{} r v + 2 r v / 3 = {}_\Delta P $$

- where r is the radius of the bubble, $\dot{r} = dr/dt$ is its derivative with respect to time, $\ddot{r} = d^2 r/dt^2$ is second derivative with respect to time, v is density of the liquid, and ΔP is the pressure difference that drives the bubble expansion. The form of the inertial terms on the left-hand side is a result of transformation of spherical three-dimensional geometry to the single radial variable. An improvement by Plesset in 1949 [22] took into consideration liquid viscosity ν and surface tension

$$ r\ddot{} r v + 2 r v / 3 = P_L - \frac{4 \dot{r} \nu}{r v} - \frac{2 \sigma}{r} - P_\infty $$
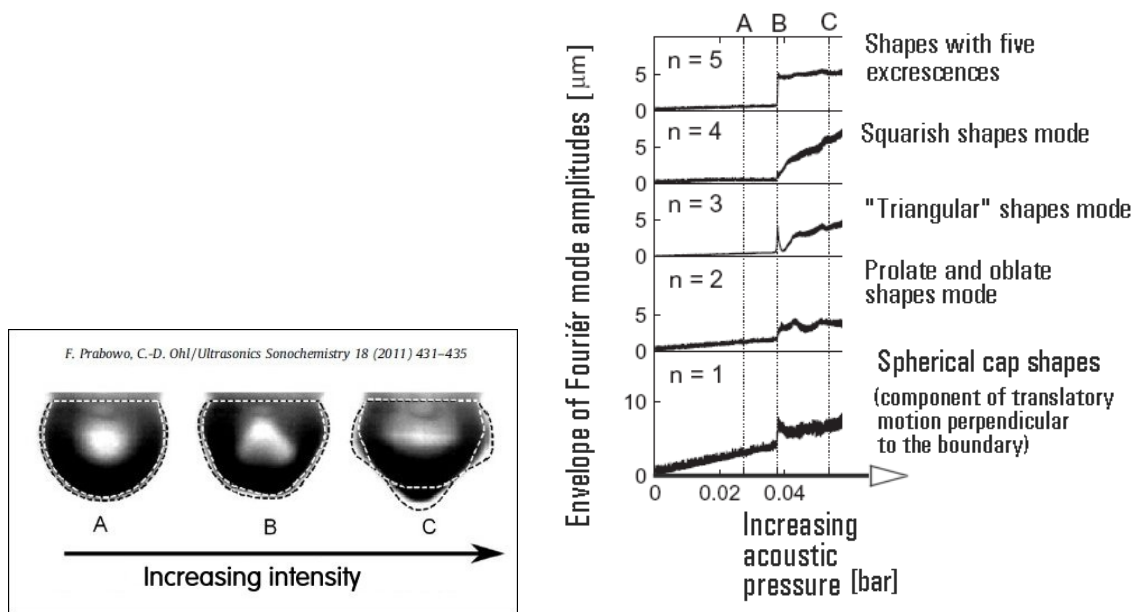
Fig. 30 (Left) Video images from [8] show the multimode vibration of a pendant bubble exposed to intense acoustic excitation.

Fig. 31 (Right) Amplitudes of the departures from the quiescent bubble shape decomposed into the five modes of increasing complexity (from n = 1 to n = 5) in ref.[8]. The letters A, B and C represent the various intensities, corresponding to Fig. 30.

When a polytropic gas law is used to evaluate the liquid pressure at the bubble wall, the contributions of surface tension σ, and vapour pressure are included, this equations receives the form in which it is still called Rayleigh-Plesset [10] equation. More advanced models are proposed and used, such as the Gilmore model incorporating sound radiation into the liquid and van der Waals hard core law accounting for incompressible volume inside the bubble. Yet another is the Keller-Miksis model featuring retarded time. All these models were developed for investigations of processes involving very high pressure changes, such as encountered in, e.g., cavitation in hydraulic machinery. Apart from this importance for practical application, these models tend to reflect interesting bubble behaviour form the theoretical point of view: the strong non-linearity leads to unusual character of the oscillation – with long expansion phase and steep collapse. Under some conditions a series of afterbounces is found after each expansion and, even strange attractor behaviour [10].

Much less have been studied the oscillatory behaviour with the bubble losing its spherical geometry, which is the object of interest in the current project. Of course, this is a much more demanding problem, since it is no more described by means of the single spatial variable (as is r in the cases retaining the sphericity). Also a number of possible spatial modes of the vibration increases. One of the few exisiting references is [8] from which is taken the information in Figs. 30 and 31. Object of the study there were five basic oscillation modes. Significantly, once the excitation has reached a certain level (labelled B in Figs. 30 and 31), amplitudes of some of these modes began to increase so much that the excrescences on the bubble surface were observed to get the character of jets leaving the bubble (and later forming satellites). No reference was found in which this process in bubbles was followed up to that stage, but the phenomenon was studied in the closely related case of a drop. As seen in Fig. 32, the object of investigations was a very low p case of sessile drop, sitting on tom of a piezoelectric vibrator. As the intensity of the vibration was gradually increased, the first effect observed on the drop surface was creation of waves distributed along the bubble meridian – at various levels of the surface inclination angle φ of the drop. More resisting and therefore requiring more intense excitation exhibited the azimuthal waves in the subsequent mode. The superposition of the azimuthal and axisymmetric waves has led to appearance of a number of local excrescence peaks. With the excitation intensity further increased, the heights of the peak tips above the basic bubble shape became relatively very large. This process has finally led to the complete fragmentation: the surface tension acting on the peaks tended to turn them into

small satellites, separated from the original large bubble. Although there is at this stage no positive documentation about it, the author believes that this effect of formation of many satellites is the explanation of the previously already observed [5, 6, 7] fragmentation phenomenon achieved by the action of a fluidic oscillator in the air supply into the growing sessile bubble.
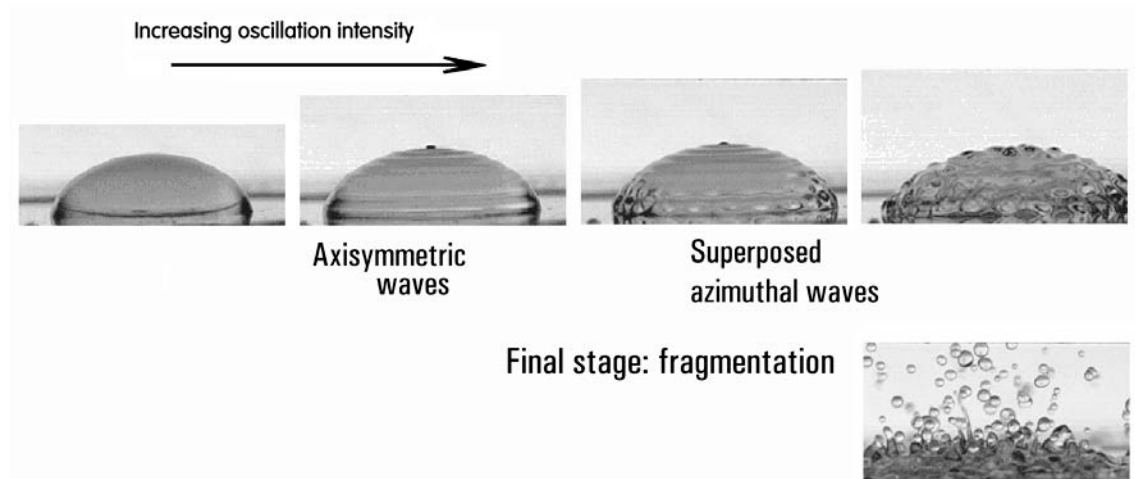
Fig. 32 Video images of an excited sessile drop from ref. [9]: increasing intensity of vibration leads first to axisymmetric waves on the drop surface, then to superimposed azimuthal waves with excrescences of growing amplitude. In the final stages the drop decomposes.

5. Experimental investigations at the Institute of Thermomechanics

In the starting phase of the research project, the aim was to demonstrate the existence of microbubbles and, in the case of positive findings, to obtain some basic data about their formation. The experimental facility was built so as to make possible more detailed investigations later. In spite of all
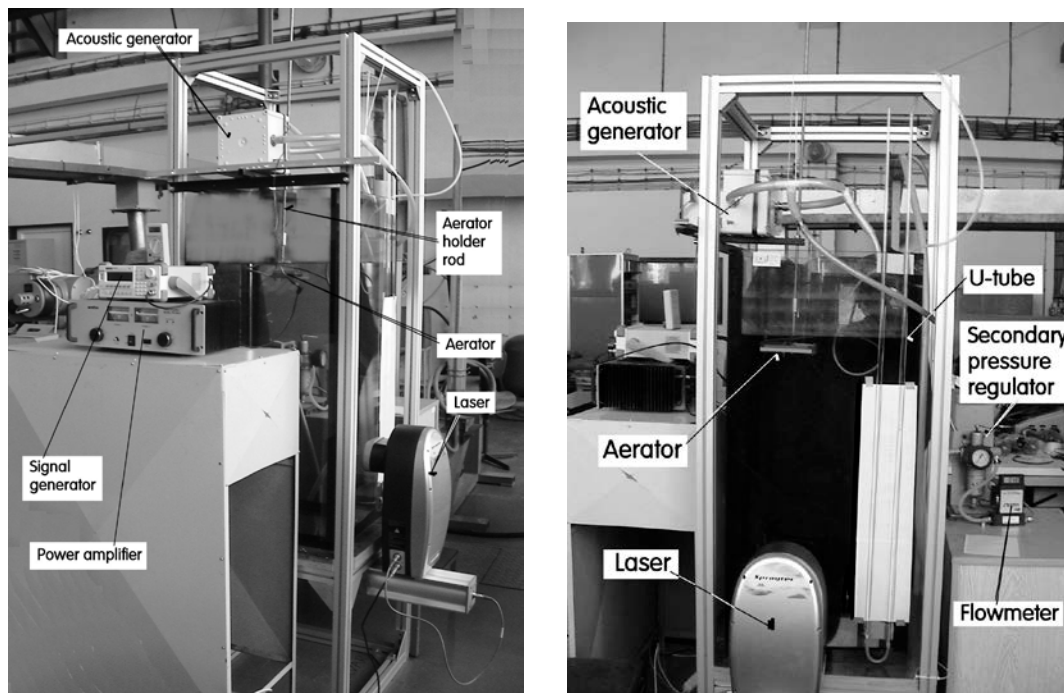
Fig. 33 (Left) Fig. 34 (Right) Author's experimental facility for studies of microbubble formation at the Institute of Thermomechanics. The main component is a thick-walled glass vessel of ground-plan size 500 mm x 500 mm and height 1100 mm. The wall thickness is 18 mm.

advantages offered by the no-moving-part fluidics, it was decided not to use them in the initial stages and to replace them by an electrodynamic acoustic generator. The reasons for this step were as follows:

1) Development of a fluidic oscillator at this stage of their development is by no means easy. Some authors still speak about fluidics as being a " black art".

2) Typical property of many fluidic oscillators (in particular of those with feedback loop channels, is the strong dependence of the frequency of generated oscillation on the flow rate.

Both aspects would unduly complicate the main aim of the investigations in their initial stages.

The core part of the experimental facility, as it is shown in the photographs Fig. 33 and 34 is a rectangular water tank with glass walls. An aerator is immersed into the water, being held on a vertical rod from above. This makes possible future investigation (not attempted at this stage) of the influence of hydrostatic pressure by moving the aerator lower. Since the fluidic oscillator to be used later has its output signal usually consisting from two components – a steady flow component and the alternating flow - this character of the signal was also applied here. The steady component uses air from the Institute's compressed air system, passing first through the primary pressure regulator (at the entrance into the laboratory) and then finely adjusted by the secondary regulator at the test stand. The alternating flow was provided by an acoustic generator, using as the electrodynamic driver a standard mass-produced loudspeaker. The loudspeaker is fixed inside a box with the air inflow both in front of as well as behind the speaker membrane. This avoids excessive membrane displacement by the steady-flow pressure. The box is positioned near the top of the water tank. The loudspeaker is supplied with electric signal of adjustable frequency (and also waveshape – again a feature which is not yet tested: the signal in the present investigations is simply harmonic). The signal is amplified by a power amplifier.

For measurement of the size of the bubbles generated inside the water tank is used optical instrument manufactured as "Spraytec" by Malvern Instruments Ltd., U. K. – Fig. 35. The laser unit of the instrument is positioned in front of the water tank. The laser light beam it produces passes through the region in the tank containing the measured bubbles. The bubbles cause diffraction of the light and deflect a part of it to a diffraction angle dependent on the bubble size. In the receiver unit there is an array of photodiodes positioned so that a particular diode is activated only by the light deflected by a bubble of corresponding size. The main output from the instrument – apart from various other information it also offers – is the spectrum of the type presented in Fig. 36 for one of the test cases. The height of the vertical columns in the diagram indicates the percentage of the total number of bubbles which were found within the $100\ \mu m$ width of the bubble size window.

Even though the final size of the microbubbles should be obtained by the fragmentation phenomenon, it is obvious that there is a distinct advantage obtained if the fragmentation process begins with smaller-sized bubbles – i.e. with small aerator exits. As a starting point, author suggested two kinds
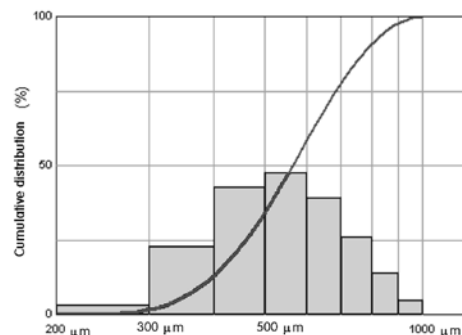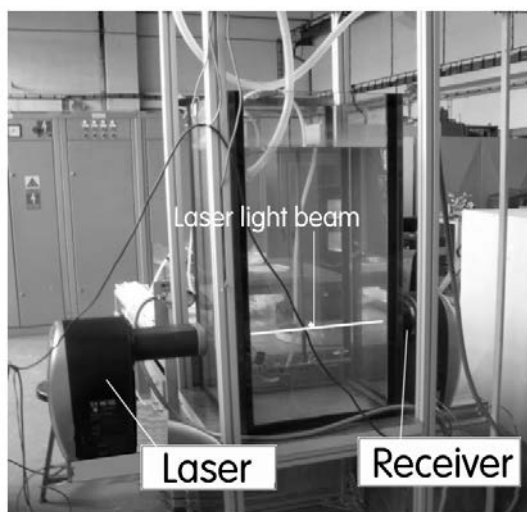
Fig. 35 (Left) The Spraytec instrument (manufactured by Malvern Instruments Ltd., U. K.) used for measurement of bubble size by evaluating diffraction of laser light.

Fig. 36 (Right) Typical Spraytec output: spectrum of populations at individual bubble size intervals and the line of cumulative distribution.
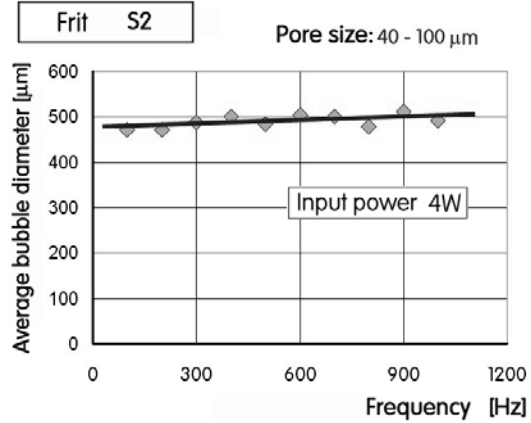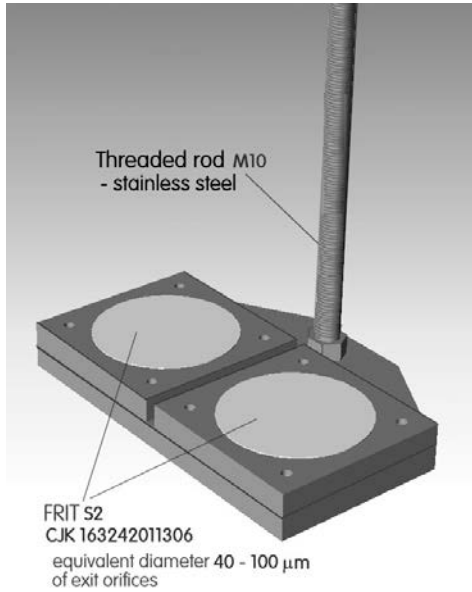
Fig. 37 (Left) The aerator model used in the tests. Originally, it contained two glass frit samples of 60 mm diameter and 5 mm thickness. Later one of the frits was replaced by a woven stainless steel mesh.
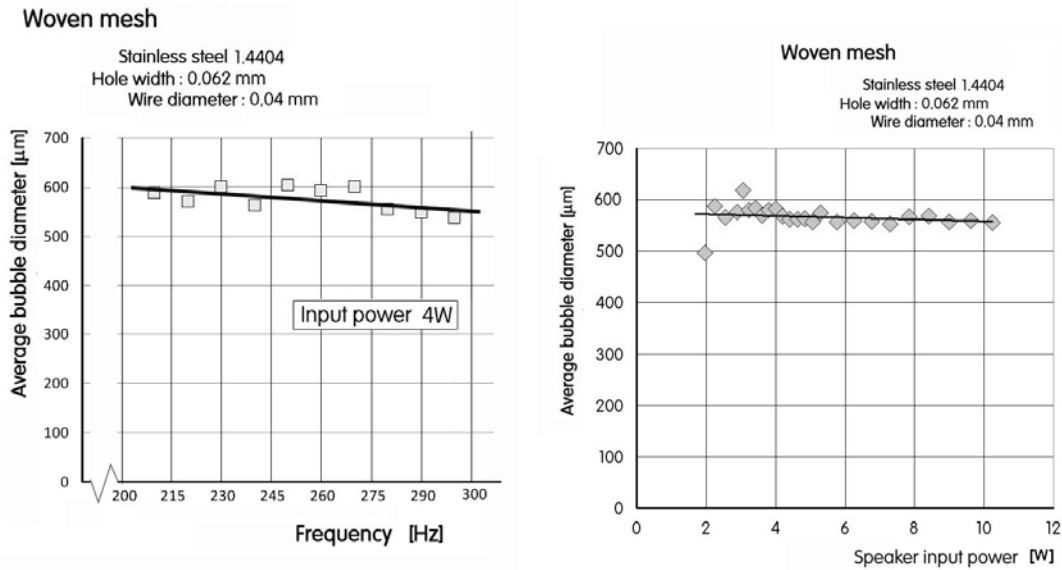
Fig. 38 (Right) Results of typical bubble size measurements: diameter of bubbles produced at the pore exits of a frit aerator as a function of oscillator frequency. Rather surprisingly, the size was found almost independent on the frequency of applied oscillation.

of active surfaces (note that the current standard aerator surface as shown in Figs. 3 and 4 was considered out of question). The first aerator model used glass frits – partially sintered glass powder – with the size of the pores given by the manufacturer unfortunately within a quite wide range from 40 μm to 100 μm. The second model was a woven mesh of stainless-steel wires. The wire diameter was 40 μm, the size of the holes between them was 62 μm. The obvious advantage of the wire mesh is the higher aerodynamic efficiency – lower pressure losses of the air flow through the pores. On the other hand, the higher aerodynamic resistance of the 5 mm thick frit may bring a certain trend to suppress the inherent instability of parallel bubble formation. Tested surfaces were in the shape of 60 mm diameter disks, fixed on a holder as shown in Fig.37.
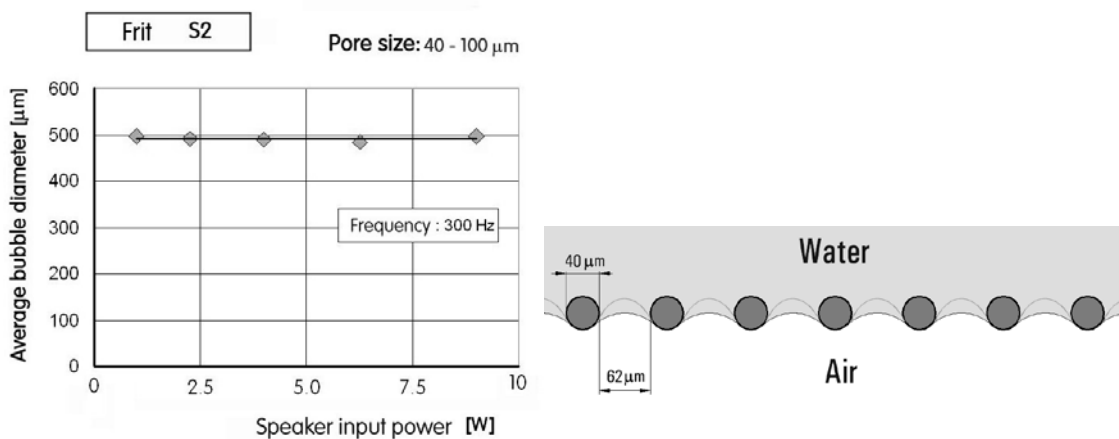
Fig. 39 (Left) Results of typical measurements of the size of microbubbles generated by the frit aerator at different settings of the loudspeaker electric driving power. Again, the size was practically invariant.

Fig. 40 (Right) Conditions on the woven steel mesh, drawn to scale. Without the acoustic excitation, the air was kept below the mesh and did not pass through. Only after drastic increase of air pressure the bubbles were formed – these, however, were then of the millimetre size. With the acoustic driving, submillimetre size microbubbles were generated even at low air pressure.

Woven mesh

Stainless steel 1.4404
Hole width : 0.062 mm
Wire diameter : 0,04 mm

Woven mesh

Stainless steel 1.4404
Hole width : 0,062 mm
Wire diameter : 0.04 mm

Fig. 41 (Left) Size of the microbubbles generated on the stainless steel mesh at various frequencies of the acoustic excitation. The bubbles were actually slightly larger than obtained with the frit – but tended to decrease with increasing frequency, which is quite in opposite to the trend seen in Fig. 38.

Fig. 42 (Right) The effect of varied driving power on the microbubble size obtained with the steel mesh. Again the bubbles are slightly larger than with the frit, but the difference is hardly significant.

The main – in fact critical – result of the tests was the established fact that the oscillation can indeed generate the sub-millimetre microbubbles.

An example of the microbubble measurements with the frit aerator is presented in Fig. 38. It is a diagram of measured average diameters of the microbubbles plotted as a function of the frequency of oscillation. What was expected was a dependence with pronounced resonance peaks. No such features were actually found: quite surprisingly there does not seem to be any particular recommendable operating frequency. There is a slight increase of the size with increasing frequency so that it may be recommended to use rather low frequency, at around $100\ \text{Hz}$. The slope of the dependence is, however small and commensurable with the data scatter.

What is certainly even more surprising is the diagram Fig. 39. In this case the frequency was kept constant and it was the power fed into the electrodynamic driver that was varied. In view of the knowledge obtained from previous experiments in [8], [9] – as presented here in Figs. 30, 31, and 32 – the fragmentation and hence much smaller bubble size was expected to appear at a certain threshold intensity magnitude. In Fig. 9, no such thing is visible. The size of the bubbles seems to be constant, irrespective of the intensity of the acoustic action.

The last illustrations, Figs. 40, 41, and 42 present the analogous results obtained with the wire mesh aerator (again in the form of a $60\ \text{mm}$ diameter disk). There is again practically no significant dependence of the average bubble diameter – neither on frequency not on power. If there were not the different values (bubble size at around $600\ \mu\text{m}$ instead of the slightly smaller $500\ \mu\text{m}$ with the frit), there would be a suspicion that the Spraytec instrument becoming stuck at a certain value it indicates. Also there is a downwards slope of the line fitted to the data in Fig. 41 (while the data in Fig. 38 suggest an upwards, positive slope.

In addition, the closer observation of the phenomena taking place at the aerator bring an interesting fact. What the acoustic action does not seem to be the expected fragmentation. Without the oscillation, the supplies air remains under the mesh. This is visually recognisable as a change in the optical properties: initially, the space under the mesh is water filled and this makes the aerator surface appearing dark. Bringing in air result in the dark colour exchanged with much lighter grey – but no bubble formation (the situation may correspond to the conceptual illustration in Fig. 4). If the acoustic excitation is then switched on, without any other change, the generation of microbubbles immediately begins. This invariably takes place at a particular spot or a few spots on the aerator surface area.

6   Interim conclusions

Microbubbles of sub-millimetre size are called for in industrial applications and the demand is increasing. Making aerator exits smaller has been already recognised as a not successful way towards making smaller bubbles, because of the inherent instability of parallel bubble formation – some bubbles grow uncontrollably while formation in other parallel exits stops. Author's experimental evidence suggests a suitable and economically viable solution is pulsating the bubbles in the process of their formation. Unfortunately a hindrance to the progress is the fact that the mechanisms by which the pulsation produces microbubbles is not yet clear. Analysis in this paper evokes as a plausible explanation the oscillatory waves that are known to form on the bubble surface and indeed may produce excrescences leading to fragmentation. Author's experimental investigations have accumulated surprising evidence of the bubble size being essentially not dependent neither on the oscillation frequency, nor on the driving power, and even not on the character of the aerator exits. This is a strange contradiction to what was expected in the fragmentation mechanism. In view of this enigmatic situation, all conclusions that may be now formulated are of only interim character.

References

[1] Levich V.G.: "Physicochemical hydrodynamics", Englewood Cliffs, N.J., Prentice-Hall, 1962

[2] Liger-Belair G, et al. : „On the velocity of expanding spherical gas bubbles rising in line in supersaturated hydroalcoholic solutions: Application to bubble trains in carbonated beverages". Langmuir, Vol. 16: p.1889, 2000

[3] Wu C., et al.: "Generation and characterisation of submicron size bubbles", Advances in Colloid and Interface Science, in Print, 2012

[4] Feng Z.C., Leal L.G.: "Nonlinear bubble dynamics", Annual Review of Fluid Dynamics, Vol. 29, p. 201, 1997

[5] Zimmerman W. B. J., Zandi M., Bandulasena H.C.H., Tesař V., Gilmour D.J., Ying K.: "Design of an airlift loop bioreactor and pilot scales studies with fluidic oscillator induced microbubbles for growth of a microalgae *Dunaliella salina*", Applied Energy, Vol. 88, p. 3357, 2011

[6] Zimmerman W.B.J., Tesař V., Bandulasena H.C.H.: „Towards energy efficient nanobubble generation with fluidic oscillation", Current Opinion in Colloid & Interface Science, Vol. 16, p. 350, 2011

[7] Zimmerman W.B. J, Tesař V.: "Bubble generation for aeration and other purposes", European Patent EP2081666, granted 19th Oct. 2011, published 26th Sept. 2012

[8] Prabowo F., Ohl C.-D.: "Surface oscillation and jetting from surface attached acoustic driven bubbles:, Ultrasonic Sonochemistry, Vol. 18, p. 431, 2011

[9] Vukasinovich B., Smith M. K., Glezer A.: "Dynamics of a sessile drop in forced vibration", Journal of Fluid Mechanics, Vol. 587, p. 395, 2007

[10] Lauterborn W., Kurz T.: "Physics of bubble oscillations", Reports on Progress in Physics, Vol. 73, p.106501, 2010

[11] Lord Rayleigh: „ On the pressure developed in a liquid during the collapse of a spherical cavity", Philosophical Mag. Ser. 6, Vol. 34, p. 94, 1917

[12] Minnaert M.: "On musical air bubbles and the sounds of running water", Philosophical Mag. Ser. 7, Vol. 16, p. 235, 1933

[13] Hanotu J., Bandulasena H.C.H., Zimmerman W.B.J.: " Microflotation performance for algal separation", Biotechnology and Bioengineering, Vol. 109, p. 1663, 2012

[14] Crum L. A., Prosperetti A.: „Non-linear oscillations of gas bubbles in liquids —an experimental interpretation of some experimental results", Journal of Acoustic Society of America, Vol. 73, p. 121, 2983

[15] Martínez-Bazán C., Rodríguez-Rodríguez J., Deane G. B., Montañes J.L., Lasheraz J.C.: "Considerations on bubble fragmentation models", Journal of Fluid Mechancs, Vol. 661, p. 159, 2010

[16] Kolmogorov, A. N.: "On the disintegration of drops in turbulent flow", Doklady Akad. Nauk, Vol.66, p. 825, 1949

[17] Qian D., McLaughlin J.B., Sankaranarayanan K., Sundaresan S., Kontomaris K.: "Simulation of bubble breakup dynamics in homogeneous turbulenc*e*", Chem. Eng. Comm, Vol. 193, p. 1038, 2006

[18] Tesař V.: "Fluidics Applied to Generation of Small Aeration Bubbles*",* Proc. of FLUCOME 2007, 9th International Symposium on Fluid Control, Measurement and Visualization, Paper 13, Tallahassee, Florida, U.S.A., September 2007

[19] Tesař V. .: "Pressure-driven microfluidics", monograph, ISBN-10: 1596931345, published by Artech House Publishers, Norwood, MA 02062 USA

[20] Laplace de (Marquis) P. S.: "Traité de Mécanique Céleste", 4th volume, 1st section (*Teéorie de l'action capillaire*) of the supplement to Book 10 (Sur divers points relatifs au systéme du monde), publ. by Cez Courier, Paris, 1806

[21] Tesař V.: "Fluidic Control of Molten Metal Flow", Acta Polytechnica - Journal of Advanced Engineering, Vol.43, p. 15 , 2003

[22] Plesset M.S., "The dynamics of cavitation bubbles", Journal of Applied Mechanics, Vol. 16, p. 277, 1949